

Cite this: *J. Mater. Chem. C*, 2017,
5, 314

The role of oxygen defects in a bismuth doped ScVO₄ matrix: tuning luminescence by hydrogen treatment

Hai-Shan Zhang,^a Fengwen Kang,^{ab} Yu-Jun Zhao,^a Mingying Peng,^a Dang Yuan Lei^b and Xiao-Bao Yang^{*a}

We have investigated the mechanism of tunable luminescence in a bismuth doped ScVO₄ matrix by using the first-principles calculations. It is found that some intrinsic defects generally exist in the matrix due to their low formation energies, while they have no remarkable effect in the optical band gap of the compound. The calculated formation energy of substitutional Bi at the Sc site is 2.0–3.3 eV lower than that of replacing V by Bi in various chemical environments. Yet, once there is an oxygen defect (vacancy) around a Bi atom, it is energetically preferable to form a defect complex, Bi_{Sc} + Va_O. Based on the calculated formation energy and the imaginary part of the dielectric function, the defect complex transfers between the neutral charge state and the 1+ charge state, which is ascribed to be responsible for the red bismuth photoemission observed in experiment. With the defect complex, tunable bismuth photoemission could be achieved by selectively controlling the content of hydrogen. Our calculations have shown that there is a passivation effect resulting from the re-padding of the oxygen defect by the hydrogen atom. This confirms the experimental observation of tunable bismuth luminescence due to the defect complex, leading to a potential facile design of other defect-controllable, micro- and nano-sized luminescent materials ranging from the visible to the near- and far-infrared spectrum.

Received 6th September 2016,
Accepted 29th November 2016

DOI: 10.1039/c6tc03880h

www.rsc.org/MaterialsC

1. Introduction

Traditional phosphors are primarily rare earth (RE) ion doped semiconductor materials with wide band-gap energies. For example, tunable luminescence from 650 nm for CaS:0.1%Eu²⁺ to 625 nm for Ca_{0.2}Sr_{0.8}S:0.1%Eu²⁺ was considered to be most promising for red phosphors,^{1,2} Y₂O₃S doped with Eu³⁺, a kind of red phosphor, has been investigated for near ultraviolet (UV) InGaN-based light emitting diodes (LEDs),^{3–5} Ba₃MgSi₂O₈ doped with 0.075 and 0.05 moles of Eu²⁺ and Mn²⁺ ions shows three emission colors: 442, 505, and 620 nm, which could be used to fabricate white LEDs,⁶ where the above-mentioned fluorescence emissions are mainly derived from the intrinsic transitions at fixed energy levels (*e.g.*, 4f → 4f for Eu³⁺ and 5d → 4f for Eu²⁺, Mn²⁺). However, RE ions, a non-renewable energy source, will run down sooner or later, showing unsustainability in the foreseeable years. Thus, researchers are encouraged

to construct alternative fluorescent materials without RE ions, by the comprehensive consideration of non-RE characteristics and material structures.

Due to its various unique physical and chemical properties, the non-RE bismuth is an excellent candidate for making up the disadvantages of RE ions. It is reported that bismuth can possess various luminescent species ranging from UV light to visible/near-infrared/even far-infrared light. As for the visible luminescence, the bismuth valences are mainly focusing on trivalent bismuth (Bi³⁺) and bivalent bismuth (Bi²⁺), in which the former is always selected as the sensitizer of RE ions for improving the RE luminescence,^{7–9} while the latter can emit either orange or red under UV/blue excitations.^{10–12} However, due to the weak luminescence, Bi²⁺ is premature to be applied in white LED illumination. In previous works about phosphors, the X-ray photoelectron spectra (XPS) of samples were compared with the XPS of typical *a*-Bi₂O₃, confirming that Bi³⁺ could stably exist in solid state compounds (Y_{*x*}Lu_{*y*}Sc_{*z*})_{1–*a*}VO₄:*a*Bi (*a* = 0–5.0%, *x* + *y* + *z* = 1).¹³ Furthermore, Bi³⁺ was present in the ScVO₄ and ScVO₃ samples for a long time during the reduction process.¹⁴ All these references can exclude the influence of Bi²⁺ ions on Bi³⁺ luminescence. That is to say, only Bi³⁺ has good potential application in white LEDs. This can be exemplified by the successful white LED fabrication based on LuVO₄:Bi³⁺ phosphors.¹⁵

^a Department of Physics & School of Materials Science and Engineering & Key Laboratory of Advanced Energy Storage Materials of Guangdong Province & The State Key Laboratory of Luminescent Materials and Devices, South China University of Technology, Guangzhou 510640, P. R. China.
E-mail: scxbyang@scut.edu.cn; Tel: +86 2087110427

^b Department of Applied Physics, The Hong Kong Polytechnic University Hong Kong, China

Extrinsic defects are particularly notable in luminescent materials. Many luminescent materials relying on different chemical-bonding environments belong to extrinsic defect-assisted materials,^{16,17} in which electronic states are created between the valence band (VB) and the conduction band (CB), for instance the carbon-based boron oxynitride phosphor.¹⁸ It is also found that if there is no appropriate extrinsic defect help, nanospheres and quantum dots (QDs) with tunable emissions (e.g., SiO₂,¹⁹ Al₂O₃,²⁰ and MoS₂^{21–23}) cannot be realized. Therefore, introducing and (or) adjusting even a quite small amount of defects can allow us to change the luminescence performance greatly. In addition, controlling the defects *via* external temperature to enhance the photoemission intensity is also reported. For example, the intensity of the LuVO₄:Bi³⁺ phosphor can reach ~1.9 times at 250 °C when compared to that at room temperature.¹⁵ It is obvious that defects have a significant influence on the luminescence properties of materials. Oxygen vacancy is a fundamental intrinsic defect in metal oxide semiconductors and may bring a crucial effect on their electronic and physicochemical properties. Bismuth oxyhalide (BiOX) (X = Cl, Br, I) with oxygen vacancies can absorb visible light and display excellent visible light photocatalytic activity, in a large part due to a new electronic peak of the Bi-6p state in the forbidden band contributed by the oxygen vacancies.^{24–27}

As the isostructural compound of LuVO₄, ScVO₄ is reported to possess the unusual red luminescence under UV excitation, which, verified by DFT results, is ascribed to the integrated contributions of the complexes produced by Bi³⁺ and the modulation of oxygen vacancy created by the replacement of Sc³⁺ with Bi³⁺.²⁸ In addition, a blue-shift of the ScVO₄:Bi³⁺ emission in a hydrogen atmosphere is expected due to new defects related to hydrogen and oxygen vacancies generated in the vicinity of the introduced Bi³⁺ ion.¹⁴ Deeper mechanisms of the unusual red luminescence and the confusing blue shift phenomenon, however, are still open questions, at least including: (i) what kind of defects are responsible for the red luminescence could be stable under different experimental conditions; (ii) how orbital energy transition triggers the red luminescence; (iii) how the hydrogen atoms diffuse and what is the exact reason for the blue-shift of the Bi³⁺ emission; (iv) whether we can effectively utilize the defects to realize the tunable luminescence from the experimental consideration; (v) which way is more suitable for us to begin with the exploration of the mutual relationship between the defect role and luminescence performance as defects are bad-controllable and hard-predictable in experiments by conventional techniques.

Enlightened by the above issues, herein we therefore carried out the relevant studies. With utilization of first-principles calculations, detailed analysis was performed by discussing the possible influence of intrinsic and extrinsic defects on the red Bi³⁺ luminescence in ScVO₄. After analyzing the formation energies with the actual Fermi energy position by charge compensation, we determined the stable defects and the defect complex Bi_{Sc} + Vac_O resulting from the substitution of an Sc atom by a Bi atom. We showed the intrinsic optical properties of blue-emitting ScVO₄ and red-emitting ScVO₄:Bi and, in combination

with the experimental observations, further evaluated the importance of oxygen defects in the tunable Bi photoemission in ScVO₄. The concept of the defect role we show here is expected to give an important implication for researchers to design and realize the tunable photoemission of crystal materials.

2. Theoretical details

The first-principles calculations were performed on the basis of the density functional theory (DFT) method, as implemented in the Vienna *ab initio* simulation package (VASP).^{29,30} The exchange correlation potential was calculated by using projector augmented wave (PAW) potentials with generalized gradient approximation (GGA) in the Perdew–Burke–Ernzerhof (PBE) format.^{31,32} To minimize the computational cost, the Bi percentage, which is comparable to the maximum nominal doping percentage (~3.0%) in ScVO₄:Bi,²⁸ was adopted in the modeling process, though the optimal Bi content corresponding to the strongest emission intensity was experimentally determined to be ~1.0%. The 2 × 2 × 2 supercell with 192 atoms was used for the calculations of vacancies. All the structures were fully relaxed with the mesh of a 1 × 1 × 1 *k*-point grid by conjugate gradient minimization, and the force criteria were 0.05 eV Å⁻¹. The *k*-point grid was increased to 2 × 2 × 2 to obtain accurate energies and optical properties with atoms fixed. To improve the calculations of electronic properties, we used the Hubbard *U* model in DFT calculations to deal with the 3d electrons for both Sc and V, where *U* and *J* values of 3.0 and 0.8 eV are adopted, respectively. The cut-off energy of the plane-wave was set to be 450 eV, achieving the energy convergence within 1 meV per atom.

The defect formation energy containing atoms α in the charge state q was calculated by means of the following equation:³³

$$\Delta H_{\text{f}}^{(\alpha,q)} = E(\alpha, q) - E(0) + \sum_{\alpha} n_{\alpha} (\Delta\mu_{\alpha} + \mu_{\alpha}^{\text{solid}}) + q(E_{\text{VBM}} + E_{\text{F}}) \quad (1)$$

where $E(\alpha, q)$ and $E(0)$ are the total energy of the supercell with and without involving defect; $\Delta\mu_{\alpha}$ is the absolute value of the chemical potential of the atom referred to its most stable phase $\mu_{\alpha}^{\text{solid}}$; n_{α} is the number of each type of defect atom; n_{α} value is -1 or +1, depending on whether one atom is added or removed, respectively; E_{VBM} represents the energy at the valence band maximum (VBM) of a defect-free system, and E_{F} is the Fermi energy relative to the E_{VBM} .

3. Experimental design and characterization

A batch of 10 g mixture powder with the nominal chemical composition of Sc_{0.99}VO₄:0.01Bi was initially synthesized in air by reacting the unpurified raw materials of Sc₂O₃ (99.99%), NH₄VO₃ (99.95%) and Bi₂O₃ (99.999%) in a tube furnace at 1100 °C for 3 hours. After 5 min intermediate grinding in an agate mortar, homogenous powder was obtained and then divided into four equal batches for the following hydrogen

atmosphere treatment. Except for one batch for comparison, the remaining three batches were treated for the same time (1 min) but at different hydrogen concentrations at 1100 °C. N_2/H_2 ratios for the three batches were set as 97.5/2.5, 95/5 and 92.5/7.5, respectively. Finally, all samples were reground again for the following photoluminescence characterization.

Static excitation and emission spectra of all samples were performed by using a high resolution FLS 920 spectrofluorometer (Edinburgh Instruments) equipped with a red-sensitive photomultiplier (Hamamatsu R928P) in a Peltier air-cooled house in single photon counting mode. To illustrate how the hydrogen atmosphere influences the relevant photoluminescence and avoids the errors as well as to understand the relationship between theoretical and experimental results, for instance the emission intensity and the atmosphere-dependent position-shift, the excitation and emission slits were fixed to be 1.5 nm and 2.0 nm, respectively. All excitation and emission spectra were performed at room temperature and corrected over the lamp intensity with a silicon photodiode and the PMT spectral response.

4. Results and discussion

4.1 Structural stability analysis

Firstly, in order to determine the stability of the intrinsic defects in blank $ScVO_4$ and the extrinsic defects caused by external Bi atom doping, all the possibilities were considered on the basis of first-principles calculations. In blank $ScVO_4$, since there is no external Bi atom doping, we have focused on the intrinsic defects ranging from Sc, V, and O vacancies (V_{AcSc} , V_{AcV} , and V_{AcO}) to Sc, V, and O interstitial defects (Sc_i , V_i , and O_i) and to antisite defects caused by cation substitution of Sc by V or V on Sc (namely, Sc_V or V_{Sc}). Returning to eqn (1), one can notice that defect formation energy is exhibited as a function of $\Delta\mu_x$ and E_F . In the process of formation energy calculations, there are some thermodynamic limits on $\Delta\mu_x$ and E_F . In this case, except for maintaining the essential E_F value between E_{VBM} and E_{CBM} , in order to ensure the successful formation of $ScVO_4$ phase and, at the same time, to avoid the competitive phase formation (including the elemental solids, *e.g.*, Sc and V *etc.*), the chemical potentials $\Delta\mu_x$ need to further meet the following requirement:

$$\Delta\mu_{Sc} + \Delta\mu_V + 4\Delta\mu_O = \Delta H_f(ScVO_4) \quad (2)$$

$$m\Delta\mu_{Sc} + n\Delta\mu_V + p\Delta\mu_O \leq \Delta H_f(Sc_mV_nO_p) \quad (3)$$

$$\Delta\mu_{Sc} \leq 0, \quad \Delta\mu_V \leq 0, \quad \Delta\mu_O \leq 0 \quad (4)$$

With the constraints of eqn (2)–(4), the calculated chemical potentials of Sc, V and O could form a chemical region, as shown in the shaded area of Fig. 1. Based on the equilibrium conditions, one can easily grasp the growth conditions of the $ScVO_4$ phase. Herein, we have selected three typical chemical potential points M (anion-rich/cation-poor (I), $\Delta\mu_{Sc} = -9.49$ eV, $\Delta\mu_V = -7.67$ eV, $\Delta\mu_O = 0$), N (anion-rich/cation-poor (II), $\Delta\mu_{Sc} = -8.91$ eV, $\Delta\mu_V = -8.25$ eV, $\Delta\mu_O = 0$) and P (anion-poor/cation-rich, $\Delta\mu_{Sc} = -6.01$ eV, $\Delta\mu_V = -3.40$ eV, $\Delta\mu_O = -1.94$ eV). After that, we obtain the formation energies of the corresponding

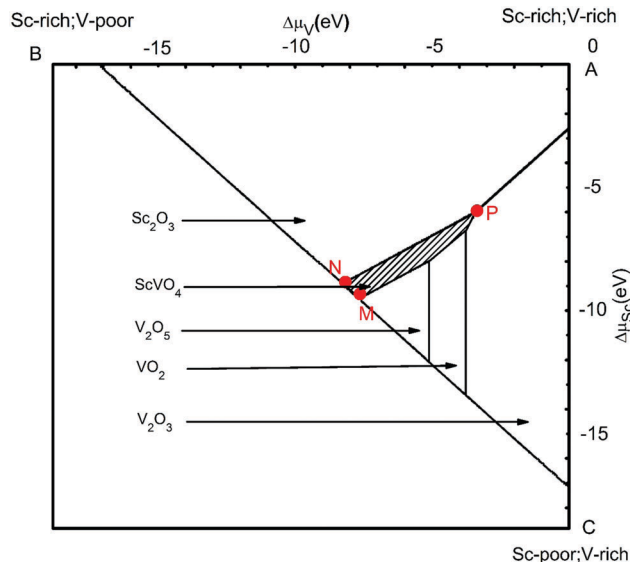


Fig. 1 Phase diagram of the $ScVO_4$ stability region (shaded part) and the competing phases in the $(\Delta\mu_{Sc}, \Delta\mu_V)$ plane.

intrinsic defects as a function of the Fermi level at chemical potentials M, N, and P (see Fig. 2(a)–(c)). For each defect, only the charge state with the lowest formation energy is indicated at each value of the Fermi level. The kink points shown in the formation energies curves correspond to charge state transition levels. Here, the defect concentrations are calculated at the experimental sample preparation temperature (1400 K) with self-consistent Fermi levels, carrier concentrations and defect concentrations.^{34,35} Subsequently, the Fermi level at room temperature (300 K) is further calculated with the fixed defect concentrations, while their charge states are allowed to be relaxed under charge neutrality conditions. As shown in Fig. 2, there are several stable defects in blank $ScVO_4$, *i.e.*, V_{Sc} in 1+, 0 charge states; O_i in 0, 1– charge states and V_{AcO} in 1+, 2+ charge states as well as Sc_V in the 2– charge state.

After analysing the intrinsic defects, we begin to evaluate the extrinsic defects caused by external Bi atom doping. Experimentally, upon excitation with UV light, Bi^{3+} can emit red/orange luminescence in $ScVO_4$.²⁸ Due to the close cationic radii and the same charges between Bi^{3+} and Sc^{3+} , when Bi atoms are built in a $ScVO_4$ matrix, two kinds of possible defects induced by the Bi_{Sc} and Bi_V substitutions and other defect complexes should be considered accordingly. In order to prevent the generation of some Bi-related compounds (*e.g.*, Bi_2O_3 , $BiVO_3$, $BiVO_4$), the following constraints are used:

$$m\Delta\mu_{Bi} + n\Delta\mu_V + p\Delta\mu_O \leq \Delta H_f(Bi_mV_nO_p) \quad (5)$$

Upon utilization of eqn (5) and the above chemical potentials of V and O at M, N and P points, the chemical potentials of Bi at M, N, and P points are calculated to be -3.93 , -3.35 and -0.45 eV, respectively. According to the three chemical potentials (see Fig. 2(a)–(c)), we provide the formation energy of several defects as listed in Table 1, and the Fermi level is determined by the charge balance analysis. The formation energy of Bi_V

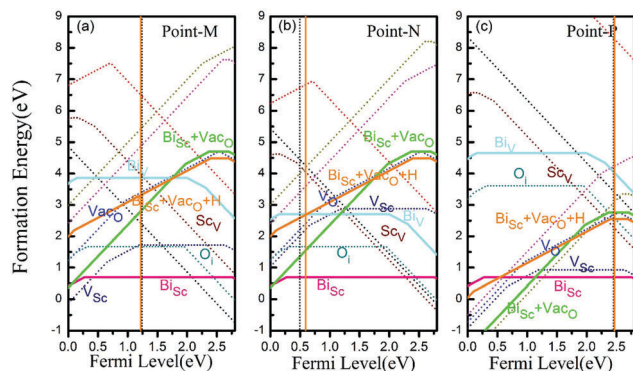


Fig. 2 The formation energies of all possible intrinsic defects (dash line) and extrinsic defects (solid line). The extrinsic defects contain Bi ions in charge states $q = -2, -1, 0, +1$ and $+2$ under the respective chemical potentials (namely, the phase diagram of point-M (a), point-N (b) and point-P (c), see Fig. 1). The vertical lines indicate the equilibrium Fermi energy position $E_{F_i}^{eq}$ with the intrinsic defects only (dash line) and the extrinsic defects containing Bi ions are considered (solid line). The defect formation energy calculations are based on the chemical potentials at points M, N and P shown in Fig. 1.

is 2.01–3.3 eV greater than that of Bi_{Sc} , which indicates that the external Bi atoms have an extremely strong energetic preference to substitute the Sc sites. In addition, the Fermi level position illustrates that the neutral charge defect Bi_{Sc} is very stable in the present chemical potential environment. Previous DFT calculations have told us that the single defect of Bi_{Sc} has no significant effect on the optical properties of ScVO_4 ,²⁸ but Bi atom incorporation can easily give rise to forming the defect complex $\text{Bi}_{\text{Sc}} + \text{Vac}_\text{O}$. Differing from the previous results, as clearly shown in Fig. 2(a)–(c), our work further shows that under the chemical potential environment of metal-poor/oxygen-rich points M and N, the defect complex $\text{Bi}_{\text{Sc}} + \text{Vac}_\text{O}$ can be stabilized in the 2+ charge state; yet, once under the chemical potential environment of metal-rich/oxygen-poor point P, the charge state of the defect complex $\text{Bi}_{\text{Sc}} + \text{Vac}_\text{O}$ is 0, with its formation energy of 2.76 eV (Table 1).

If the above oxygen vacancies we calculated can indeed influence the Bi^{3+} luminescence, then we introduce a hydrogen atom to fill one generated oxygen vacancy to passivate Vac_O . After carefully inspecting the formation energies of the defect complex $\text{Bi}_{\text{Sc}} + \text{Vac}_\text{O} + \text{H}$ (also see Fig. 2(a)–(c)) and all possible chemical potential environments, it is found that the defect complex $\text{Bi}_{\text{Sc}} + \text{Vac}_\text{O} + \text{H}$ is stable in the 1+ charge state. Similar to the case of $\text{Bi}_{\text{Sc}} + \text{Vac}_\text{O}$, the neutral defect complex $\text{Bi}_{\text{Sc}} + \text{Vac}_\text{O} + \text{H}$ is preferable to exist in the chemical potential environment

Table 1 The formation energy of listed defects at points M, N and P in the chemical potential environment; superscripts are the stable charge states of defects under charge equilibrium conditions (unit eV)

	Sc_V	V_Sc	O_i	Vac_O	Bi_{Sc}	Bi_V	$\text{Bi}_{\text{Sc}} + \text{Vac}_\text{O}$	$\text{Bi}_{\text{Sc}} + \text{Vac}_\text{O} + \text{H}$
Point-M	3.95^{2-}	2.41^0	1.67^0	3.39^{1+}	0.70^0	3.87^0	2.81^{2+}	3.31^{1+}
Point-N	4.04^{2-}	2.23^{2+}	1.67^0	2.42^{1+}	0.70^0	2.71^0	1.56^{2+}	2.69^{1+}
Point-P	2.23^{2-}	0.93^0	2.55^{1-}	2.71^{1+}	0.70^0	4.00^{2-}	2.76^0	2.55^0

of metal-rich/oxygen-poor point P and the formation energy is 2.55 eV (Table 1). Of course, it has to be noted here that the chemical potential of hydrogen μ_H is the energy per H atom of the hydrogen molecule.

4.2 Dielectric function $\epsilon_2(\omega)$ analysis

It is known that the line shape of the dielectric function can reflect the optical properties of all materials. Hence, we draw the imaginary dielectric function $\epsilon_2(\omega)$ patterns of bulk ScVO_4 with and without defects, as shown in Fig. 3(a). In Fig. 3(a), the defect-related line shapes of $\epsilon_2(\omega)$ are similar to that of bulk ScVO_4 . In view of the low formation energies, the intrinsic defects could generally exist while the optical band gap of the compound is not changed, which indicates that there is light absorption at 3.0 eV. This further illustrates that the intrinsic defects have no effect on the luminescence of bulk ScVO_4 . The inset of Fig. 3(a) shows the partial density of states (PDOS) of bulk ScVO_4 . Due to the strong coupling between V-3d and O-2p

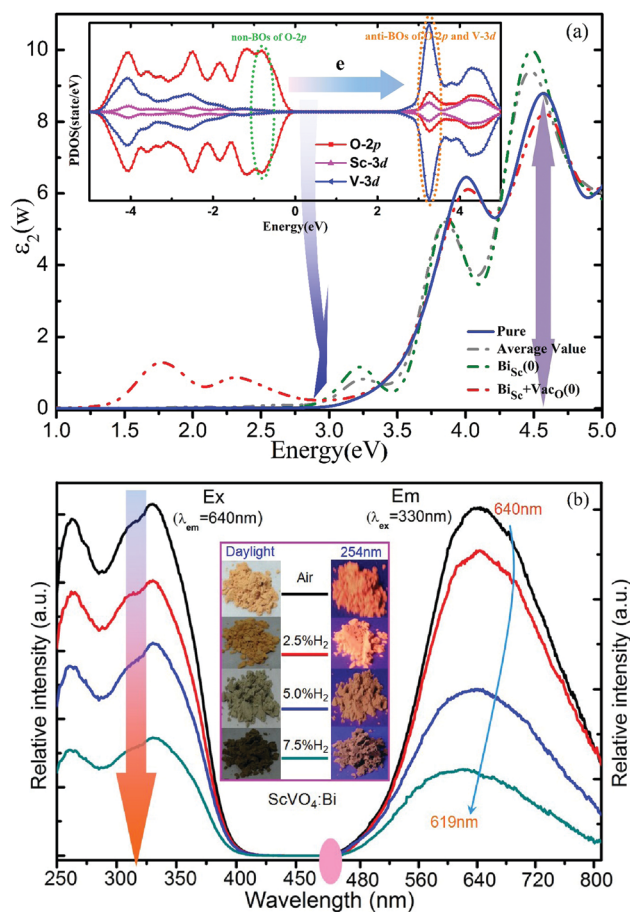


Fig. 3 (a) Calculated imaginary part of the dielectric function $\epsilon_2(\omega)$ of bulk ScVO_4 and stable defects; the grey dashed line denotes the average value of all intrinsic defects, $\text{Bi}_{\text{Sc}} + \text{Vac}_\text{O}(1+, 2+)$ and $\text{Bi}_{\text{Sc}} + \text{Vac}_\text{O} + \text{H}(0, 1+)$; the inset is the calculated PDOS of bulk ScVO_4 with per atom and per orbital contributions. (b) Excitation and emission spectra ($\lambda_\text{em} = 640$ nm, $\lambda_\text{ex} = 330$ nm) of $\text{ScVO}_4:0.01\text{Bi}$ samples treated in air and three different N_2/H_2 ratios of 97.5/2.5, 95/5 and 92.5/7.5; the inset shows the digital photographs under 254 nm excitation.

orbitals, the VBM and the CBM are contributed by the O 2p non-bonding orbitals (non-BOs) and the e anti-bonding orbitals (anti-BOs) of O-2p and V-3d, respectively. The electron transitions from the VBM to the CBM correspond to the light absorption edge that begins with 3.0 eV. Furthermore, it is obvious that there is an absorption peak around 4.6 eV, which is also why we adopt 260 nm UV light as the excitation source in the experiment.

When considering the extrinsic defects caused by Bi atom doping, the absorption edge of the dominant neutral defect Bi_{Sc} was found to be slightly lower than that of bulk ScVO_4 , which is consistent with the previous results.^{35,41} However, two peaks in the energy of 1.8 eV and 2.3 eV emerge in the $\varepsilon_2(\omega)$ line shape of the neutral defect complex $\text{Bi}_{\text{Sc}} + \text{Vac}_{\text{O}}$, indicating a valence change from 0 to 1+. We ascribe this valence change to the red Bi^{3+} luminescence in ScVO_4 . When one hydrogen atom was introduced to passivate the Vac_{O} , one can see the line shape of $\varepsilon_2(\omega)$ is the same as bulk ScVO_4 (see Fig. 3(a)). Note that, the line shapes of $\varepsilon_2(\omega)$ of all intrinsic defects, $\text{Bi}_{\text{Sc}} + \text{Vac}_{\text{O}}(1+/2+)$ and $\text{Bi}_{\text{Sc}} + \text{Vac}_{\text{O}} + \text{H}(0/1+)$, have no obvious differences. In order to express Fig. 3(a) as clearly as possible, we apply the average value of $\varepsilon_2(\omega)$ here.

4.3 Experimental confirmation

Following the above theoretical analysis, we will confirm the influence of defects on Bi luminescence. A facile experiment has been designed for $\text{ScVO}_4:\text{Bi}$ to verify the influence of the possible oxygen defects on Bi^{3+} luminescence by treating three equal amounts of $\text{ScVO}_4:\text{Bi}$ compounds in three different hydrogen atmospheres. The content of hydrogen gas is changed by controlling the N_2/H_2 ratio. Since the compounds are easily reduced by too high H_2 content or long treatment time, we set the reducing treatment time to one minute and three N_2/H_2 ratios to 97.5/2.5, 95/5 and 92.5/7.5. Our purpose is first to obtain three different reducing gas gradients and then, with the designs, to acquire three different concentrations of oxygen defects accordingly, although we cannot exactly know how much the defects have been produced. The experimental treatment design is slightly different from the previous work where fixing the N_2/H_2 ratio (95/5) but changing the treatment time is adopted.¹⁴ It is observed in the experimental results that as the hydrogen treatment concentration is increased, the excitation and emission intensities are decreased and, meanwhile, the photoemission position gradually moves toward a higher energy direction from 640 nm to 619 nm (see Fig. 3(b)). Unlike the photoemissions, the excitations do not seem to be affected by this reducing treatment, leaving the excitation shapes unchanged. The photoemission change can be reflected by the digital images of samples under a 254 nm UV lamp excitation (see Fig. 3(b) (inset)). Increasing the hydrogen concentration gradually turns the initial bright-yellow-red into dim-yellow. More than that, due to the phase conversion from ScVO_4 to ScVO_3 and the increment of photoemission energy resulting from V_{O} generation, hydrogen treatment can turn the colour of the $\text{ScVO}_4:\text{Bi}^{3+}$ sample from yellow to gray back. Since doping of ScVO_3 with Bi cannot give rise to luminescence, interaction of Bi^{3+} ions and oxygen vacancies in the ScVO_4 matrix is therefore preferably

presumed to be responsible for the experimental excitation and emission spectra as well as color variations, although the intensity is decreased as the reducing concentration is increased.

Considering the reducing influence of the H_2 atmosphere in the Bi charge state and the Bi^{2+} orange/red colors under the UV/blue excitations, the present luminescence we observed may be from Bi^{2+} , instead of Bi^{3+} . However, Bi^{2+} has its own unique spectral features, namely, three excitation (or absorption) bands resulting from the transitions of ${}^2\text{P}_{1/2} \rightarrow {}^2\text{P}_{3/2}(1)$, ${}^2\text{P}_{1/2} \rightarrow {}^2\text{P}_{3/2}(2)$ and ${}^2\text{P}_{1/2} \rightarrow {}^2\text{S}_{1/2}$ and one orange/orange-red/red emission band that correspond to the transition of ${}^2\text{P}_{3/2}(1) \rightarrow {}^2\text{P}_{1/2}$. The excitation and emission of typical Bi^{2+} doped phosphors have been reported in our previous works.^{10,36,37} Furthermore, according to our present and previous results,^{13,14,28,38,39} we can find that no matter how we change the experimental conditions for instance the H_2 atmosphere treatment, the change in temperature and the substitution of different sites in ScVO_4 by different ions, unique spectral features of Bi^{2+} are not detectable. Conversely, after considering various possibilities of our theoretical stimulations and the well matching XPS positions between typical $\alpha\text{-Bi}_2\text{O}_3$ and $\text{ScVO}_4:\text{Bi}^{3+}$ samples,¹⁴ we can confirm that Bi^{3+} could stably exist in ScVO_4 and ScVO_3 samples for a long time during the present Bi^{3+} reduction process and therefore the possible influence of Bi^{2+} ions on luminescence that we investigated can be excluded.

4.4 Bond length and electronic structure consideration

The bond length analysis and DOS calculations were employed to calculate the electronic structure of the doped system and understand its optical properties and interatomic interactions. Fig. 4 and 5 show a series of local atomic models fully relaxed in the xz plane and DOS calculation results. In a pure ScVO_4 structure, every Sc atom has eight neighbouring O atoms, with the distances of Sc–O 2.38 Å and 2.14 Å, respectively. The distance between the V and the four nearest neighbouring O atoms is always 1.72 Å (Fig. 4(a)). In addition, the V–O covalent bonds are stronger than Sc–O ionic bonds. Furthermore, taking

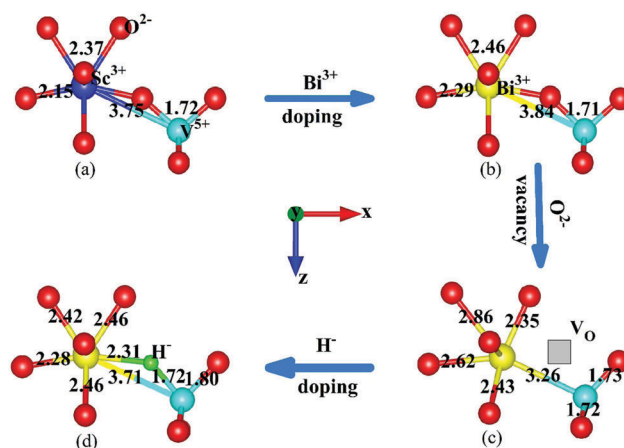


Fig. 4 Fully relaxed atomic models of bulk ScVO_4 (a), replacement of Sc by Bi (b), neutral defect complex $\text{Bi}_{\text{Sc}} + \text{Vac}_{\text{O}}$ (c) and neutral defect complex $\text{Bi}_{\text{Sc}} + \text{Vac}_{\text{O}} + \text{H}$ (d).

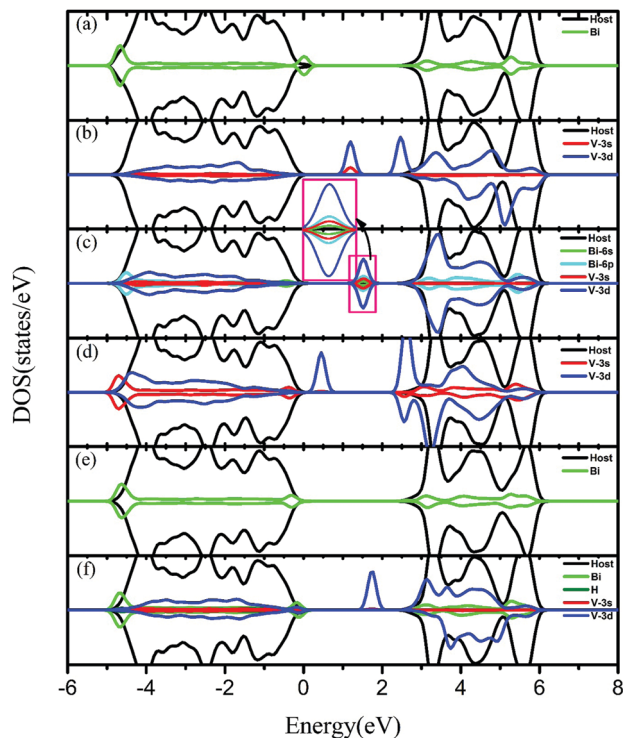


Fig. 5 Density of states of replacement of Sc with Bi in the ScVO_4 host (a), an isolated oxygen vacancy (b), an defect complex $\text{Bi}_{\text{Sc}} + \text{Vac}_{\text{O}}$ in the 0 charge state (c), 1+ charge state (d), 2+ charge state (e), and the neutral charge state $\text{Bi}_{\text{Sc}} + \text{Vac}_{\text{O}} + \text{H}$ (f). The black lines describe the density of states of bulk ScVO_4 , and color lines indicate the density of states of the impurity atoms.

the view of the charge state and the corresponding cationic radius (*i.e.*, $R_{\text{V}^{5+}} (0.54 \text{ \AA}) < R_{\text{Sc}^{3+}} (0.75 \text{ \AA}) < R_{\text{Bi}^{3+}} (1.0 \text{ \AA})$ ⁴²) into consideration, it is easy to explain the reason why Bi is more likely to replace the Sc atom relative to V. As a consequence, when replacing Sc with larger Bi, the distances of the Bi–O bond are extended to 2.4 Å and 2.31 Å, respectively, slightly longer than those of Sc–O, and the distances of the V–O bond are reduced to 1.71 Å (Fig. 4(b)). All these are due to the fact that the Bi–O bond is a little weaker than the Sc–O bond. As a result, the substitution defect Bi_{Sc} could induce a slight upward shifting of the VBM, and thus reduce the band gap to 2.6 eV, as shown in Fig. 5(a). It does not seem to be necessary to generate oxygen vacancies from the charge compensation consideration when Bi^{3+} is substituted for Sc^{3+} . However, Shahid and his co-workers have already confirmed that intrinsic Vo could exist in ScVO_4 .^{40,41} Moreover, compared with the Sc–O bond, the weaker Bi–O bond dissociates the oxygen atom near the introduced Bi atom forming a defect complex $\text{Bi}_{\text{Sc}} + \text{Vac}_{\text{O}}$ further. In an isolated Vac_{O} defect, a perfect ScVO_4 crystal leaves three dangling bonds which are derived from the coupled Sc-3d state, V-3s, and 3d, and the defect levels drop much below the CBM, as illustrated in Fig. 5(b). However, as seen in Fig. 2(a)–(c), the neutral state of isolated intrinsic defect Vac_{O} is not stable in any chemical potential environment. In other words, when there is one Vac_{O} in the system, the dangling bonds derived from the Sc and V atoms around the oxygen vacancies cannot form a localized state, and they would exist in the form of delocalized electrons.

Fig. 4(c) shows the defect complex $\text{Bi}_{\text{Sc}} + \text{Vac}_{\text{O}}$ that contains a nearest-neighbour Bi_{Sc} and Vac_{O} . To be the most stable defect, a class of defect complexes is involved with two isolated defects separated at different distances. From the previous analysis, the defect complex $\text{Bi}_{\text{Sc}} + \text{Vac}_{\text{O}}$ may exist in the neutral state at the chemical potential point P (oxygen-poor/metal-rich). In comparison with the point defect Bi_{Sc} in $\text{Bi}_{\text{Sc}} + \text{Vac}_{\text{O}}$, the distance between Bi and the second nearest neighbour V reduces from 3.84 Å to 3.26 Å. From Fig. 5(c), the neutral $\text{Bi}_{\text{Sc}} + \text{Vac}_{\text{O}}$ occupies the defect levels in the band gap contributed by Bi and V atoms. As for the model of $[\text{Sc}/\text{Bi} \cdots \text{O} \cdots \text{V}]$, due to the existence of more active Bi valence electrons, the direct coupling between Bi and V orbitals can make the deep donor levels more stable, which is important for the optical properties of the structure. Therefore, the transition between Bi-6s and Bi-6p orbitals contributes to the absorptions (1.5–2.0 eV) within the near-infrared and red ranges (Fig. 3(a) and 5(c)). Moreover, since the coupling between V-3d and Bi-6s, 6p orbitals could break the symmetry of the crystal, it will abrogate the transitions forbidden between V-3d orbitals. Thus, the optical absorption curve exhibits the absorption peaks within 2.0–2.2 eV (Fig. 3(a)). Interestingly, the donor defect complex $\text{Bi}_{\text{Sc}} + \text{Vac}_{\text{O}}$ can lose an electron to be in the 1+ charge state and, at this time, the impurity levels in the band gap mainly resulted from the V atom contribution, as shown in Fig. 5(d). Because the cancellation of the orbital coupling between Bi-2s, 2p and V-3d, there is a slight drop in the orbital energy levels of the V atom. And what is more, owing to the transition forbidden between the V-3d orbitals which locate in the band gap and the conduction band, it only emerges as a very weak light absorption at the beginning of 2.5 eV (Fig. 3(a)). When the defect complex $\text{Bi}_{\text{Sc}} + \text{Vac}_{\text{O}}$ changes to be in the 2+ charge state, the impurity levels located in the band gap disappear (Fig. 5(e)), showing the same optical band gap as that of pure ScVO_4 (Fig. 3(a)).

In the light of the qualitative analysis, the above discussions can allow us to construct the feasible model to explain the red photo-emission of Bi^{3+} in the ScVO_4 matrix. Under p-type conditions, the defect complex $\text{Bi}_{\text{Sc}} + \text{Vac}_{\text{O}}$ will be stable in the 2+ charge state, which allows it to act as a compensating centre with low formation energy. At this time, the formation energy of 1+ and 0 charge states are increasing in turn. In contrast, under n-type conditions, where E_{F} is near the bottom of the conduction band, the $\text{Bi}_{\text{Sc}} + \text{Vac}_{\text{O}}$ may exist in the 0 charge state. In both cases, the luminescence may result from the transfer of the $\text{Bi}_{\text{Sc}} + \text{Vac}_{\text{O}}$ defect center from the 0 charge state to the 1+ charge state, corresponding to the valence state transition of the Bi ions from 3+ to 2+.

The above discussion is just the case of oxygen vacancies; when treating the $\text{ScVO}_4:\text{Bi}$ compound in the reducing atmosphere, hydrogen may enter into the matrix. In this case, it naturally drives us to try to fill oxygen vacancies in the H atom. It is shown in Fig. 4(d) that the H atom we introduced localizes at the position of Vac_{O} after a full structural relaxation, which is consistent with our prediction. The distances of $\text{H} \cdots \text{Bi}$ and $\text{H} \cdots \text{V}$ are 2.31 Å and 1.72 Å, respectively, which are very close to the distances of $\text{O} \cdots \text{Bi}$ (2.29 Å) and $\text{O} \cdots \text{V}$ (1.71 Å) in the isolated defect Bi_{Sc} (Fig. 4(b)). Hence, the DOS diagram also

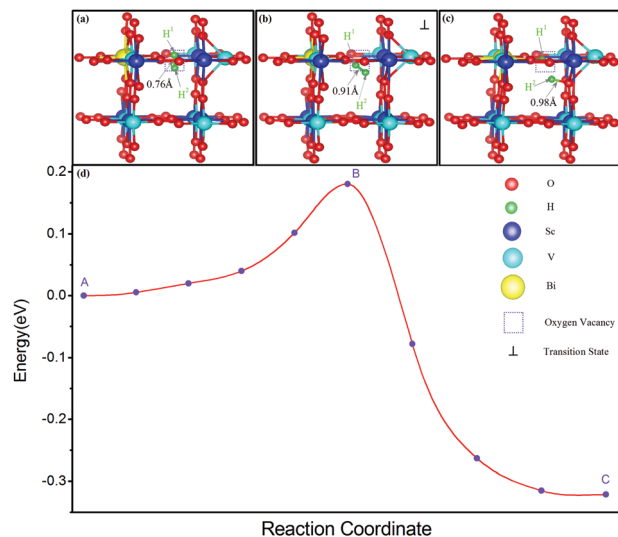


Fig. 6 Reaction pathway for the dissociative of H_2 molecule in the oxygen vacancy. Structures A, B and C are initial, transition and final states shown in (a), (b) and (c), respectively, which are all marked in reaction energy profile (d).

considers the process of $Bi_{Sc} + Vac_O$ and $Bi_{Sc} + Vac_O + H$ cases (Fig. 5(c) and (f)). It is easily understandable that the role of the H atom is to couple with partial dangling bonds, the results of which can drive the valence electron orbitals of Bi atoms that previously locate within the band gap to bond with the orbitals of the H atom and then drop the hybrid orbitals down to the position near the VBM. Of course, one can note that the defect levels derived from the V-3d orbitals remain located in the band gap. Due to the forbidden transition between the V-3d orbitals, the remaining defect levels therefore show no effect on the optical properties (Fig. 3(a)).

4.5 Reaction pathway of H_2 molecule dissociation in an oxygen vacancy

To verify whether the H_2 molecule can decompose into H atoms in experiment, we have also calculated the barrier of H_2 molecule dissociation in an oxygen vacancy (Vac_O), using the climbing image nudged elastic band (CI-NEB) technique.⁴² The energy profile of this reaction pathway is shown in Fig. 6(d), where 8 images are interpolated linearly from state A to state C. The initial state A is a H_2 molecule located in V_O as shown in Fig. 6(a). As the reaction progresses, the system will reach a transition state B (Fig. 6(b)) with an associated barrier of 0.18 eV, in which the H–H separation has been lengthened to 0.91 Å. At the end of this reaction pathway, the system reaches the final state C (Fig. 6(c)), in which the H_2 molecule has been dissociated, with one hydrogen atom located in the Vac_O , and the other bonded with an oxygen atom forming a hydroxyl. The calculation results show that the barrier of H_2 molecule dissociation in Vac_O is as low as 0.18 eV, which is a good proof for the above analysis.

5. Summary and outlook

In this work, we theoretically investigated the stabilities and photoelectrical properties of the intrinsic defects of bulk $ScVO_4$

and extrinsic defects caused by Bi atom doping. The results showed that the intrinsic defects have no effect on the luminescence of bulk $ScVO_4$. Since the substitutional Bi_{Sc} defect is energetically preferable, one Vac_O around the Bi atom will be created, forming the defect complex $Bi_{Sc} + Vac_O$. As a consequence, the orange/red Bi^{3+} luminescence is generated. More than that, with re-filling the Vac_O by a hydrogen atom, the passivation effect emerges. This is confirmed experimentally by the blue-shifting of photoemission positions when $ScVO_4:Bi$ was treated in the reducing hydrogen atmosphere. Our results can potentially serve as a facile implication for the development of defect-controllable luminescence materials, by making use of crystal defects.

Acknowledgements

This work was supported by the NSFC (Grant No. 11474100, 51322208, 51672085), the Guangdong Natural Science Funds for Distinguished Young Scholars (Grant No. 2014A030306024, S20120011380), the Foundation for Innovative Research Groups of the National Natural Science Foundation of China (Grant No. 51621001) and Natural Science Foundation of Guangdong Province of China (Grant No. 2016A030312011), the Department of Education of Guangdong Province (Grant No. 2013gjh0001), and the Key Program of Guangzhou Scientific Research Special Project (Grant No. 201607020009). The computer times at the National Supercomputing Center in Guangzhou (NSCCGZ) are gratefully acknowledged.

References

- Z. Qiu, T. Luo, J. Zhang, W. Zhou, L. Yu and S. Lian, *J. Mater. Chem. C*, 2015, **3**, 9631–9636.
- C. Guo, D. Huang and Q. Su, *Mater. Sci. Eng., B*, 2006, **130**, 189–193.
- C. Guo, L. Luan, C. Chen, D. Huang and Q. Su, *Mater. Lett.*, 2008, **62**, 600–602.
- T. W. Chou, S. Mylswamy, R. S. Liu and S. Z. Chuang, *Solid State Commun.*, 2005, **136**, 205–209.
- Z. Wang, H. Liang, L. Zhou, H. Wu, M. Gong and Q. Su, *Chem. Phys. Lett.*, 2005, **412**, 313–316.
- J. S. Kim, P. Jeon, J. Choi, H. Park, S. Mho and G. Kim, *Appl. Phys. Lett.*, 2004, **84**, 2931–2933.
- F. W. Kang, Y. Zhang and M. Y. Peng, *Inorg. Chem.*, 2015, **54**, 1462–1473.
- S. Yan, J. Zhang, X. Zhang, S. Lu, X. Ren, Z. Nie and X. Wang, *J. Phys. Chem. C*, 2007, **111**, 13256–13260.
- F. W. Kang, Y. Hu, H. Wu, G. Ju, Z. Mu and N. Li, *J. Rare Earths*, 2011, **29**, 837–842.
- M. Y. Peng, N. Da, S. Krolkowski, A. Stiegelschmitt and L. Wondraczek, *Opt. Express*, 2009, **17**, 21169–21178.
- M. Y. Peng and L. Wondraczek, *Opt. Lett.*, 2010, **35**, 2544–2546.
- M. Y. Peng, B. Sprenger, M. A. Schmidt, H. Schwefel and L. Wondraczek, *Opt. Express*, 2010, **18**, 12852–12863.

- 13 F. W. Kang, M. Y. Peng, X. Yang, G. Dong, G. Nie, W. Liang, S. Xu and J. Qiu, *J. Mater. Chem. C*, 2014, **2**, 6068–6076.
- 14 F. W. Kang, Y. Zhang, L. Wondraczek, J. Zhu, X. Yang and M. Y. Peng, *J. Mater. Chem. C*, 2014, **2**, 9850–9857.
- 15 F. W. Kang, M. Y. Peng, Q. Zhang and J. Qiu, *Chem. – Eur. J.*, 2014, **20**, 11522–11530.
- 16 Q. Dai, M. E. Foley, C. J. Breshike, A. Lita and G. F. Strouse, *J. Am. Chem. Soc.*, 2011, **133**, 15475–15486.
- 17 M. Shang, C. Li and J. Lin, *Chem. Soc. Rev.*, 2014, **43**, 1372–1386.
- 18 W. N. Wang, T. Ogi, Y. Kaihatsu, F. Iskandar and K. Okuyama, *J. Mater. Chem.*, 2011, **21**, 5183–5189.
- 19 A. M. Jakob and T. A. Schmedake, *Chem. Mater.*, 2006, **18**, 3173–3175.
- 20 C. Lin, M. Yu, Z. Cheng, C. Zhang, Q. Meng and J. Lin, *Inorg. Chem.*, 2008, **47**, 49–55.
- 21 H. Lin, C. Wang, J. Wu, Z. Xu, Y. Huang and C. Zhang, *New J. Chem.*, 2015, **39**, 8492–8497.
- 22 S. Tongay, J. Zhou, C. Ataca, J. Liu, J. S. Kang, T. S. Matthews, L. You, J. Li, J. C. Grossman and J. Wu, *Nano Lett.*, 2013, **13**, 2831–2836.
- 23 H. Nan, Z. Wang, W. Wang, Z. Liang, Y. Lu, Q. Chen, D. He, P. Tan, F. Miao, X. Wang, J. Wang and Z. Ni, *ACS Nano*, 2014, **8**, 5738–5745.
- 24 Y. Huang, H. Li, M.-S. Balogun, W. Liu, Y. Tong, X. Lu and H. Ji, *ACS Appl. Mater. Interfaces*, 2014, **6**, 22920–22927.
- 25 X. Zhang, L. Zhao, C. Fan, Z. Liang and P. Han, *Comput. Mater. Sci.*, 2012, **61**, 180–184.
- 26 W. L. Huang, *J. Comput. Chem.*, 2009, **30**, 1882–1891.
- 27 W. L. Huang, *Comput. Mater. Sci.*, 2012, **55**, 166–170.
- 28 F. W. Kang, X. B. Yang, M. Y. Peng, L. Wondraczek, Z. Ma, Q. Zhang and J. Qiu, *J. Phys. Chem. C*, 2014, **118**, 7515–7522.
- 29 G. Kresse and J. Furthmüller, *Phys. Rev. B: Condens. Matter Mater. Phys.*, 1996, **54**, 11169.
- 30 G. Kresse and D. Joubert, *Phys. Rev. B: Condens. Matter Mater. Phys.*, 1999, **59**, 1758–1775.
- 31 P. E. Blöchl, *Phys. Rev. B: Condens. Matter Mater. Phys.*, 1994, **50**, 17953.
- 32 J. P. Perdew, K. Burke and M. Ernzerhof, *Phys. Rev. Lett.*, 1996, **77**, 3865.
- 33 S. Zhang, S. H. Wei and A. Zunger, *Phys. Rev. Lett.*, 1997, **78**, 4059.
- 34 C. Persson, Y. J. Zhao, S. Lany and A. Zunger, *Phys. Rev. B: Condens. Matter Mater. Phys.*, 2005, **72**, 035211.
- 35 Y. J. Zhao, C. Persson, S. Lany and A. Zunger, *Appl. Phys. Lett.*, 2004, **85**, 5860–5862.
- 36 R. Cao, M. Y. Peng and J. Qiu, *Opt. Express*, 2012, **20**, A977–A983.
- 37 L. Li, M. Y. Peng, B. Viana, J. Wang, B. Lei, Y. Liu, Q. Zhang and J. Qiu, *Inorg. Chem.*, 2015, **54**, 6028–6034.
- 38 F. W. Kang, M. Y. Peng, D. Y. Lei and Q. Zhang, *Chem. Mater.*, 2016, **28**, 7807–7815.
- 39 F. W. Kang, H. S. Zhang, L. Wondraczek, X. B. Yang, Y. Zhang, D. Y. Lei and M. Y. Peng, *Chem. Mater.*, 2016, **28**, 2692.
- 40 P. S. Shahid, J. L. Rylan, M. D. C. Lachlan and B. Mario, *J. Solid State Chem.*, 2007, **180**, 3333–3340.
- 41 P. S. Shahid, W. K. Matthew, M. D. C. Lachlan, K. M. Vladimir, K. Scott and B. Mario, *Inorg. Chem.*, 2009, **48**, 10553–10559.
- 42 G. Henkelman, B. P. Uberuaga and H. Jónsson, *J. Chem. Phys.*, 2000, **113**, 9901–9904.